Supplementary information

**Emission of biogenic volatile organic compounds from warm and oligotrophic**

**seawater at the Eastern Mediterranean**

Chen Dayan[1], Erick Fredj[2*], Pawel K. Misztal[3], Maor Gabay[1], Alex B. Guenther[4], Eran Tas[1*]

[1]Hebrew University of Jerusalem, Rehovot, Israel (chenescohen@gmail.com), [2]Lev Academic Center, Jerusalem, Israel, [3]The University of Texas at Austin, Austin, Texas, USA, [4]University of Irvine California, Irvine, California, USA

* Correspondence to:

Eran Tas, The Department of Soil and Water Sciences, The Robert H. Smith Faculty of Agriculture, Food and Environment, Hebrew University of Jerusalem, Rehovot, Israel. eran.tas@mail.huji.ac.il,

Erick Fredj, Department of Computer Science, Jerusalem College of Technology, Jerusalem, Israel, erick.fredj@gmail.com

## S1. Availability of measured data and calibration

Measured data that did not pass the quality control were discarded, and only days with complete measured data were used for the analysis, resulting in 20 days of high-quality data.

*Table S1. Excluded measured data. Presented are data availability for the analysis and the reason for and percentage of data exclusion. ***

| Reason | Percentage |
|---|---|
| Analyzed data (good data) | 21% |
| Partial measurement days | 5% |
| Poor quality | 11% |
| File writing error | 14% |
| Calibration error | 8% |
| Measurement failure | 11% |
| Blocked tube | 28% |
| Electricity failure | 2% |

*\* Note that we have also excluded from our analyses measurements between DOY 257-260, due to irregular meteorological conditions during this period, which resulted in an atypical diurnal profile shape, with no correlation between daytime T and BVOC mixing ratios (see Sect. S4).*

According to the proton transfer reaction between the $H_3O^+$ reagent ions and a VOC producing protonated molecule $RH^+$, the signals of $RH^+$ ions $[RH^+]$ at the end of the drift tube can be described as follows

$$H_3O^+ + R \rightarrow RH^+ + H_2O \qquad \text{(Eq.1)}$$
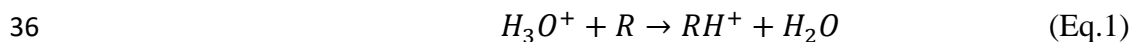
$$[RH^+] = [H_3O^+]_0\left(1 - e^{-k[R]\Delta t}\right), \qquad \text{(Eq. 2)}$$

where $k$ is the reaction rate constant, $[H_3O^+]_0$ is the signal of $H_3O^+$ ions before the reaction, $[R]$ is the number concentration of the VOC in the drift tube, and $\Delta t$ is the reaction time for $H_3O^+$ traversing the drift tube. If the proton-transfer reactions only convert a small fraction of $H_3O^+$ into protonated molecule $RH^+$, $[RH^+]$ can be approximately expressed as (de Gouw et al., 2003; de Gouw and Warneke, 2007; Lindinger et al., 1998):

$$[RH^+] \approx [H_3O^+]k[R]\Delta t\,, \qquad \text{(Eq. 3)}$$

where $[H_3O^+]$ is the signal of the $[H_3O^+]$ ions after their exit from the drift tube.

Under a small $H_3O^+$ converted fraction, Eq. (3) can be used (De Gouw et.al. 2003) to estimate the compound $[R]$ concentration from the observed ion count rates, $I(RH^+)$ for $RH^+$ ions and $I(H_3O^+)$ for $H_3O^+$ ions and the reaction rate constant $k$ as

$$[R] = \frac{1}{k\Delta t}\frac{I(RH^+)}{T(RH^+)}\left(\frac{I(H_3O^+)}{T(H_3O^+)}\right)^{-1} \qquad \text{(Eq. 4)}$$

The coefficients $T(RH^+)$ and $T(H_3O^+)$ are the transmission efficiencies for $RH^+$ and $H_3O^+$, respectively, and their values range between zero and one.

***Table S2**. Compositions of the calibration gas standards. The standard was used in the calibrations. S norm indicates the normalized sensitivity, $k_{theo}$ indicates the proton transfer reaction rate coefficients $k$ reported by (Cappellin et al., 2012), while kobs*

57     *indicates the effective proton transfer reaction rate coefficient observed during the*

58     *field campaign. See also Fig. S1 for $k_{theo}$- $k_{obs}$ regression.*

59

| Compound | S norm | m/z | $k_{theo}$ [$10^{-9}$ cm$^3$ s$^{-1}$] | $k_{obs}$ [$10^{-9}$ cm$^3$ s$^{-1}$] |
|---|---|---|---|---|
| Acetaldehyde | **18.5** | 45 | 3.17 | 3.16 |
| acetone | **22.8** | 59 | 3.32 | 3.28 |
| MVK+MACR | **21.6** | 71 | 3.30 | 2.77 |
| MEK | **25.9** | 73 | 3.28 | 3.27 |
| Benzene | **16.5** | 79 | 1.93 | 1.99 |
| Toluene | **19.8** | 93 | 2.08 | 2.16 |
| Xylene | **22.7** | 107 | 2.26 | 2.28 |
| TMB | **22.4** | 121 | 2.40 | 2.10 |
| D5 | **40.5** | 371 | 2.00 | 2.03 |

60
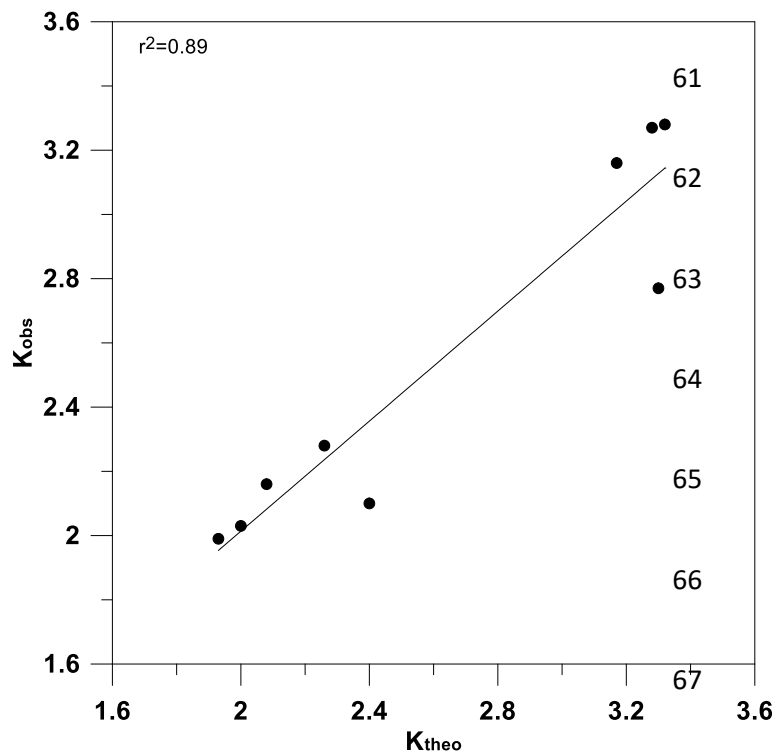
**Fig. S1**. *k_{theo}-k_{obs} regression. Presented are the k_{theo}-k_{obs} regression and the corresponding coefficient of determination (r^2).*

70
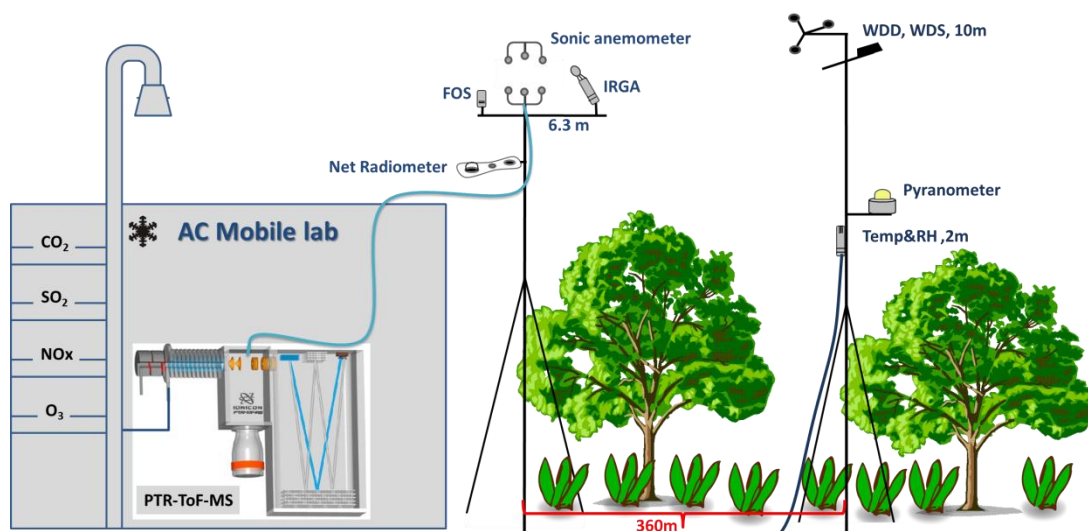
**Fig. S2.** *Schematic of the measurement setup. Eddy covariance measurements used and open path sensors at a height of 6.9 m to quantify $O_3$, $CO_2$ and $H_2O$ mixing ratios, as well as VOCs by PTR-TOF-MS, which was located in an air-conditioned mobile laboratory, together with trace gas monitors. Basic meteorological parameters were measured at a distance of 360 m, within the nature park. See Sect. 2.2 for more detailed information.*

**S2. The origin of the measured VOCs**

Fig. 3 in the main text points to elevated emission of MVK+MACR, isoprene oxidation products, from both the west and southeast. The former could indicate an isoprene origin from the sea, while the latter could suggest emission of MBO and/or isoprene. Considering the short distance from the memorial gardens (~40 m), oxidation of isoprene to both MACR and MVK is far too slow to account for the observed MVK+MACR mixing ratios. Moreover, the m87/m69 indicates elevated MBO emission from southeast, which could be attributed to emission from conifers in the memorial gardens
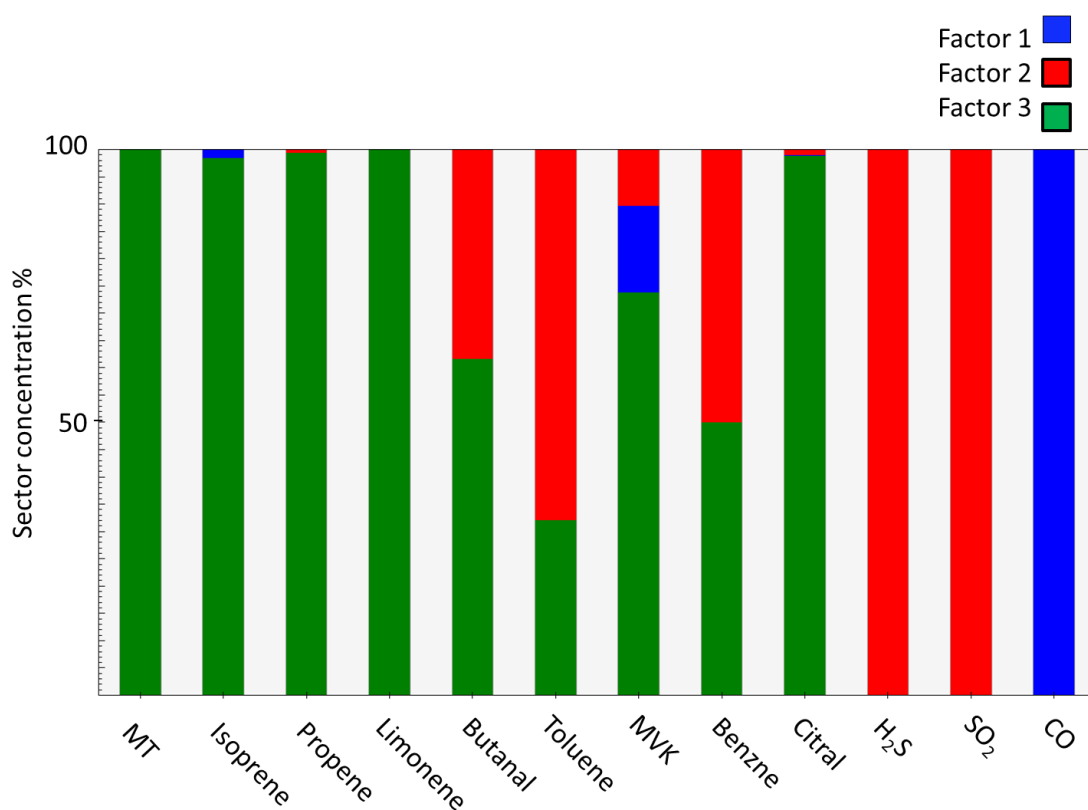


**Fig. S3.** *Example of PMF model results for August 13-14, 2015. Suggested biogenic factor in green, anthropogenic factors in red and blue.*

Luo and Yu (2010) suggested that the global contribution of oceanic emissions to MT is ~4% of that of isoprene.
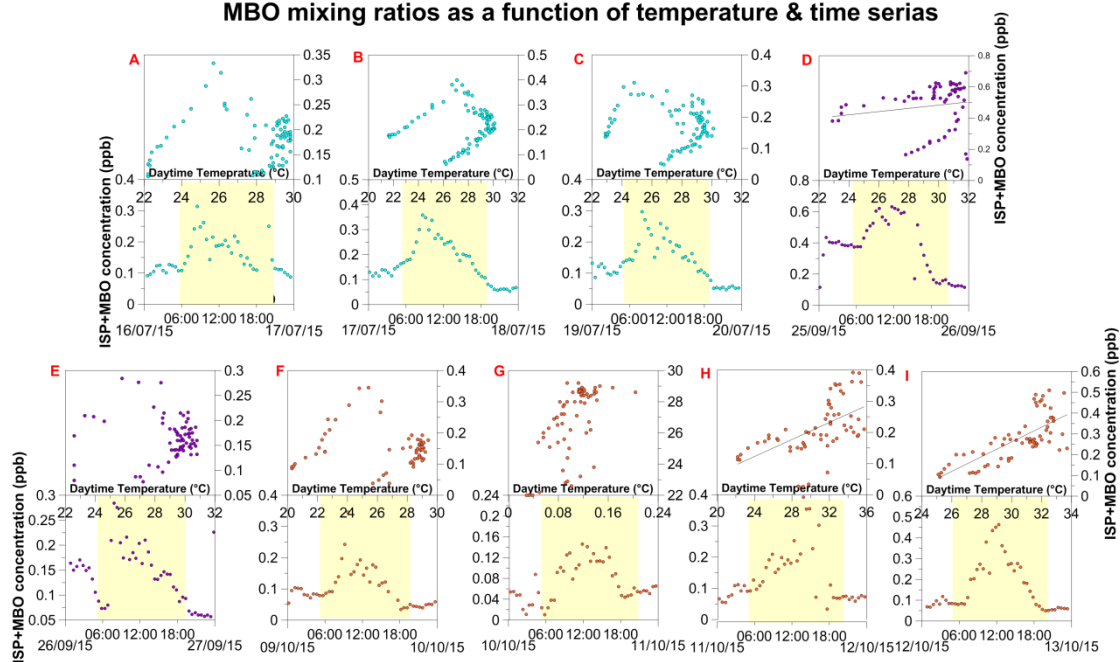
**Fig. S4.** *MBO (*m87/m96>13%*) mixing ratios diurnal average and dependence on temperature. Upper panels show regression between measured* m87/m9625>% *and T and lower panels* show m87/m96>25%. *Yellow shaded area represents daylight hours.*
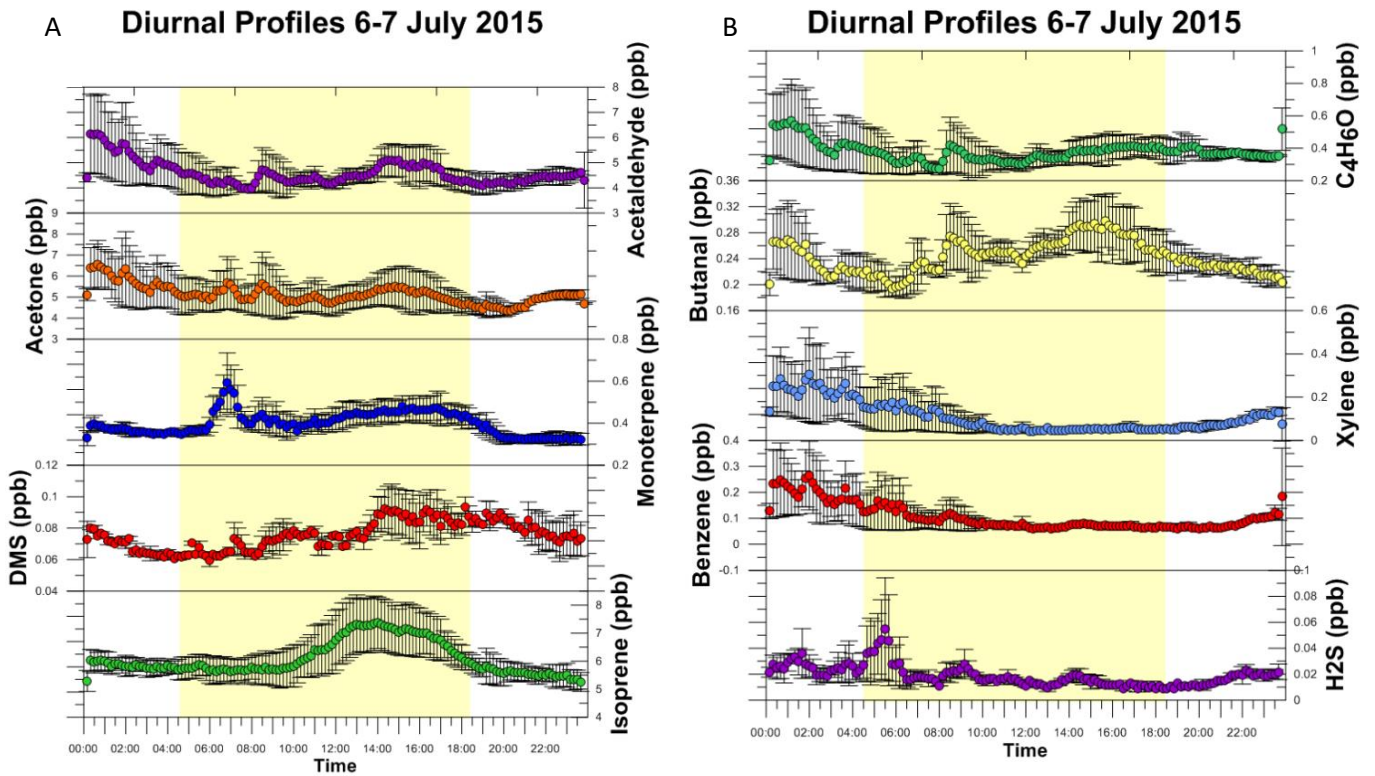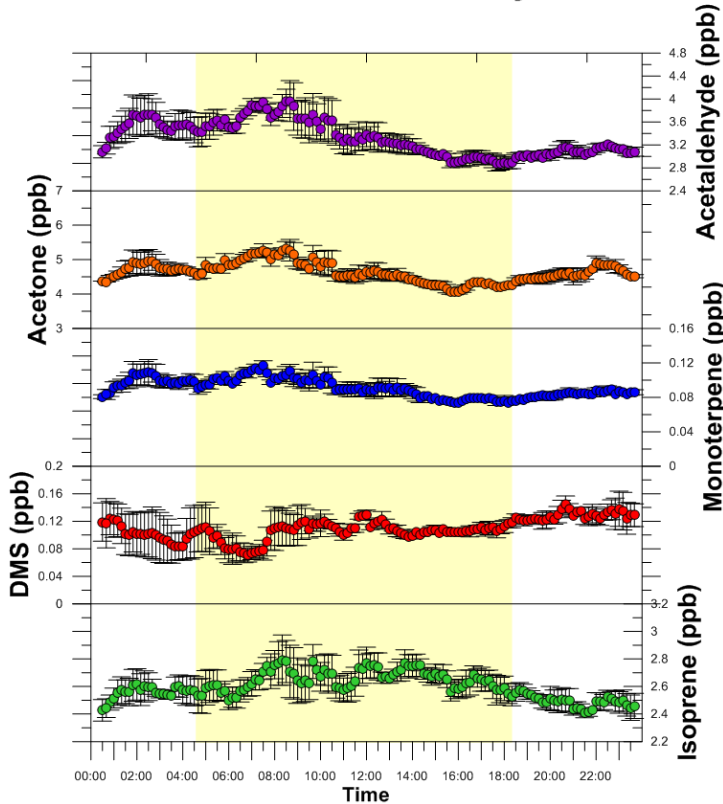
**Figure S5**. *Average diurnal profiles of BVOCs (A) and AVOCs (B) between 6-7 July, 2015.*
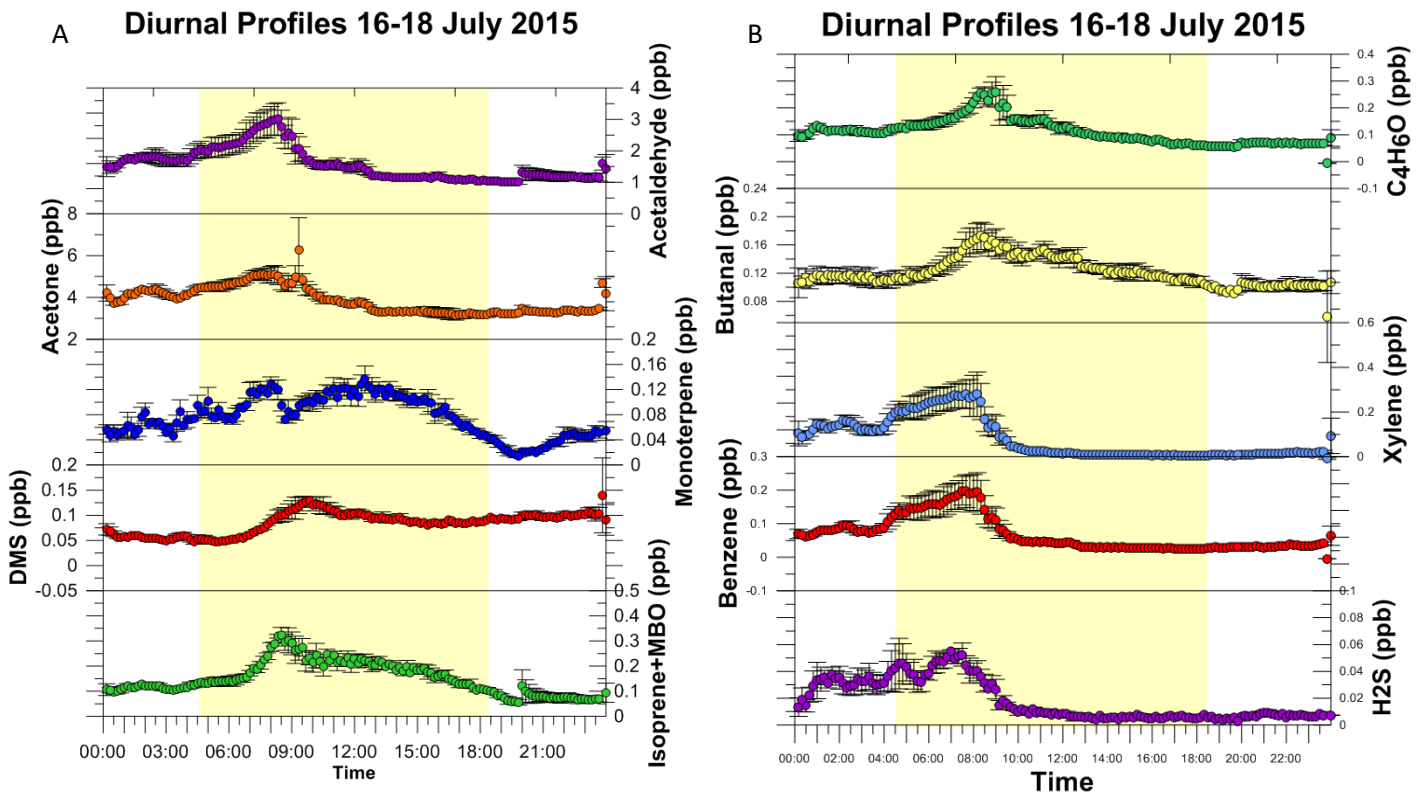


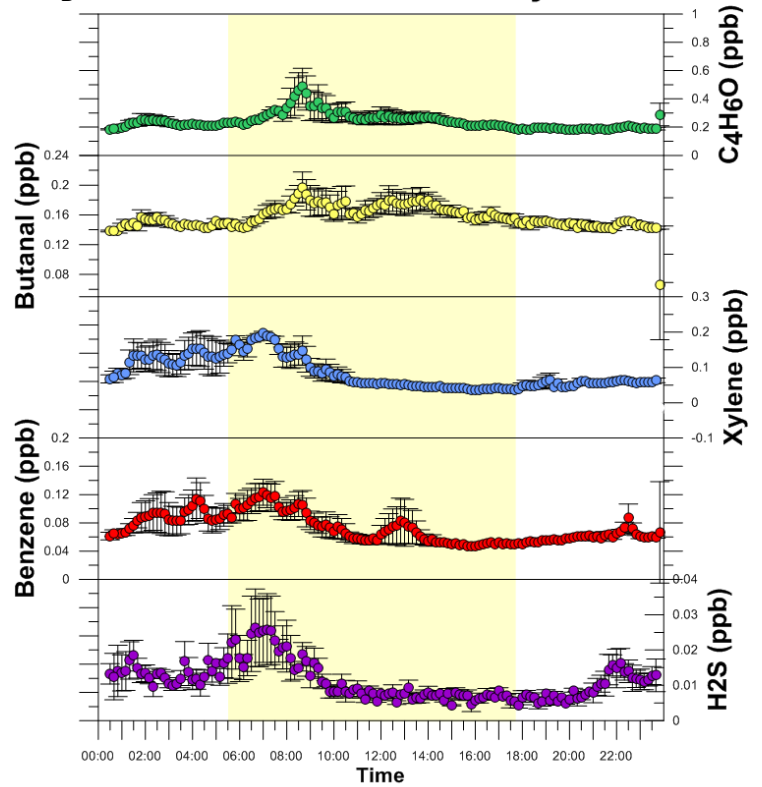**Figure S6**. *Average diurnal profiles of BVOCs (A) and AVOCs (B) between 16-18 July, 2015.*

**Figure S7**. *Average diurnal profiles of BVOCs (A) and AVOCs (B) between 24-26 July, 2015.*
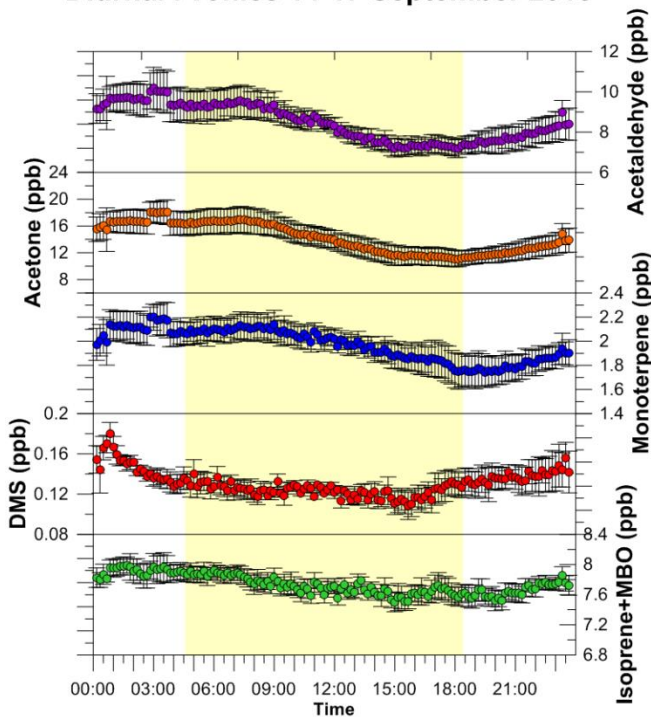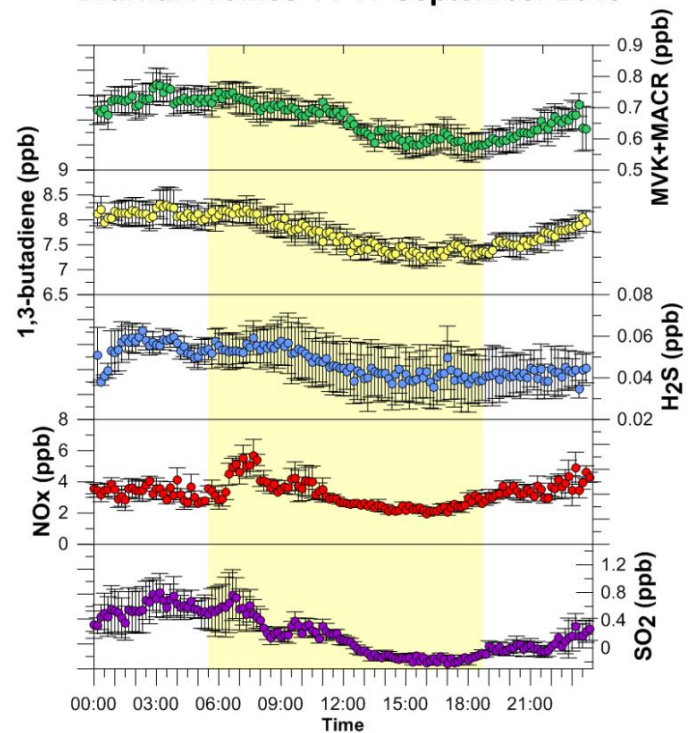


**Figure S8**. Average diurnal profiles of BVOCs (A) and AVOCs (B) between 14-17 September, 2015.

149
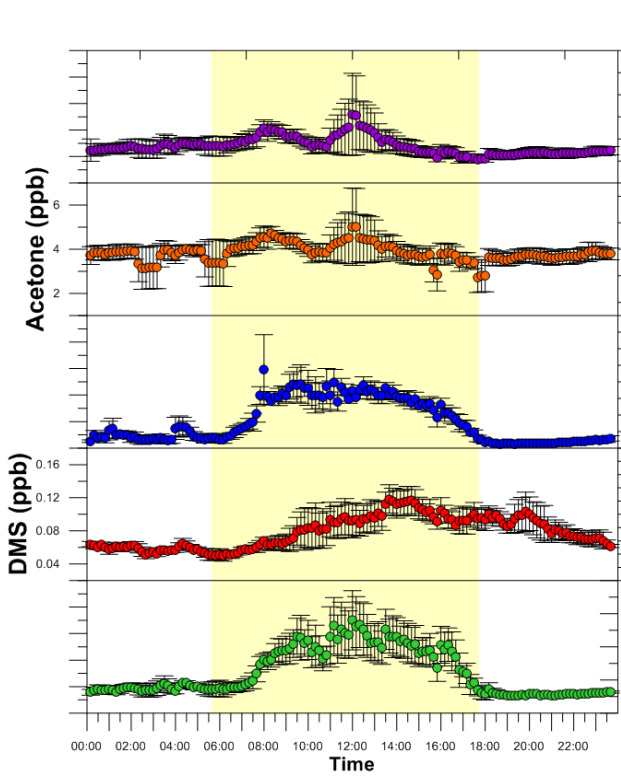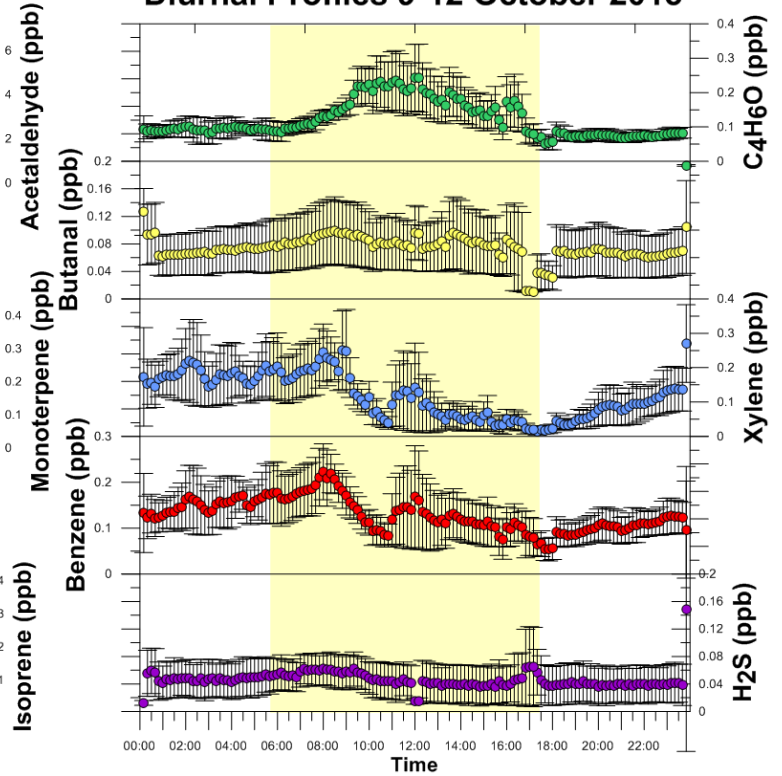
**Figure S9**. *Average diurnal profiles of BVOCs (A) and AVOCs (B) between 14-17 October, 2015.*
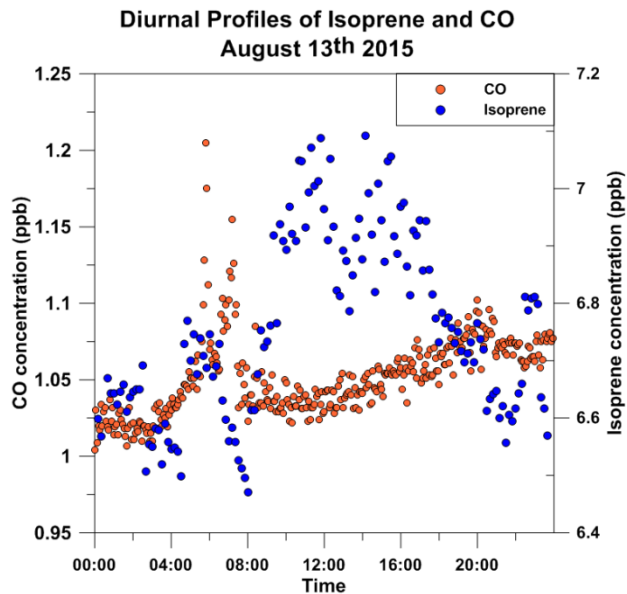


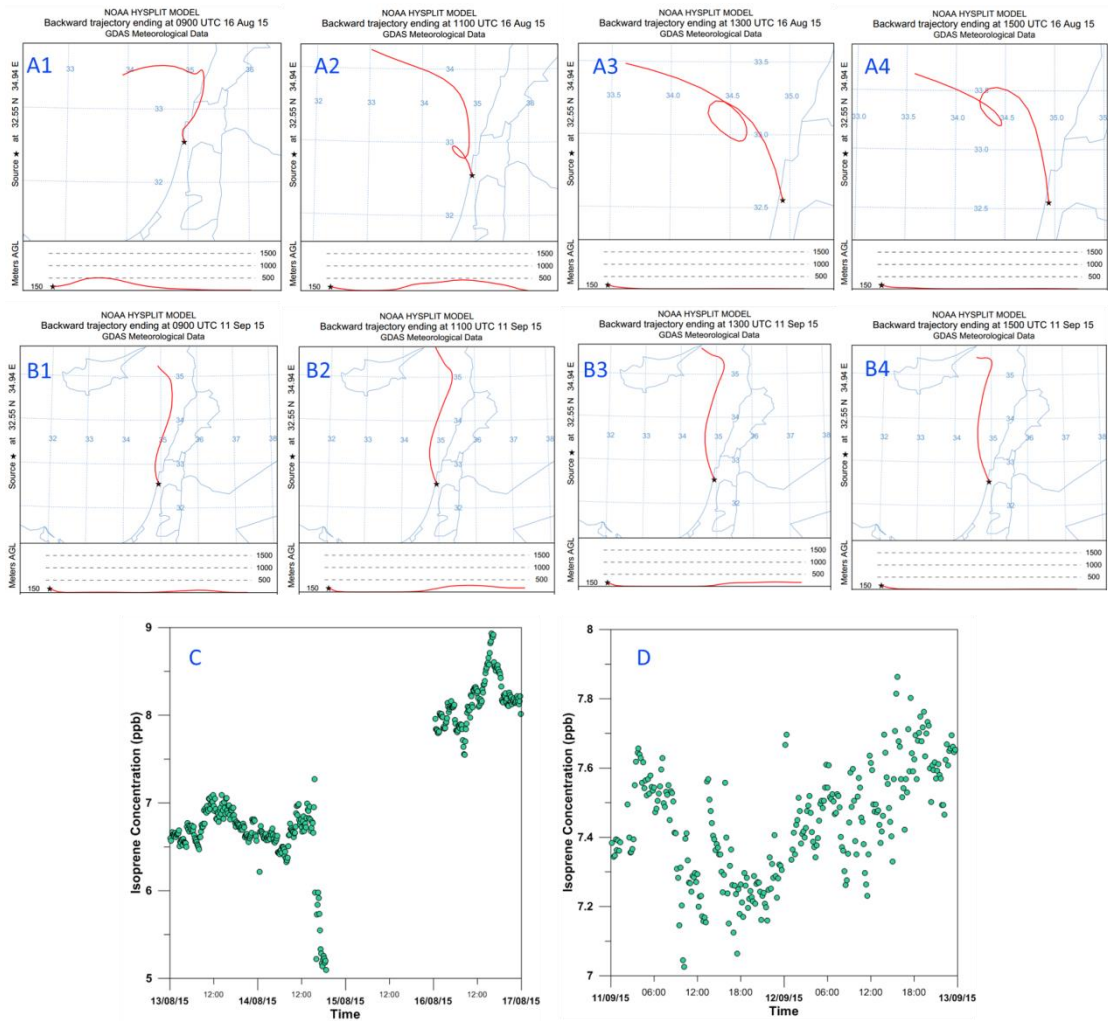**Figure S10**. *Comparison between CO and isoprene profiles during August 13, 2015.*

165

166    *Figure S11*. Backward trajectories for August 16, 2015 (A), and September 11, 2015

167    (B), for the hours 9:00 (A1, B1), 11:00 (A2, B2), 13:00 (A3, B3), 15:00 (A4, B4).

168    Isoprene time series for (C) September 11-12, 2015, and (D) August 13-16, 2015. This

169    example is used to demonstrate high MBO+isoprene mixing ratios when the

170    trajectories passed only over the Mediterranean Sea, not the aquafarms.
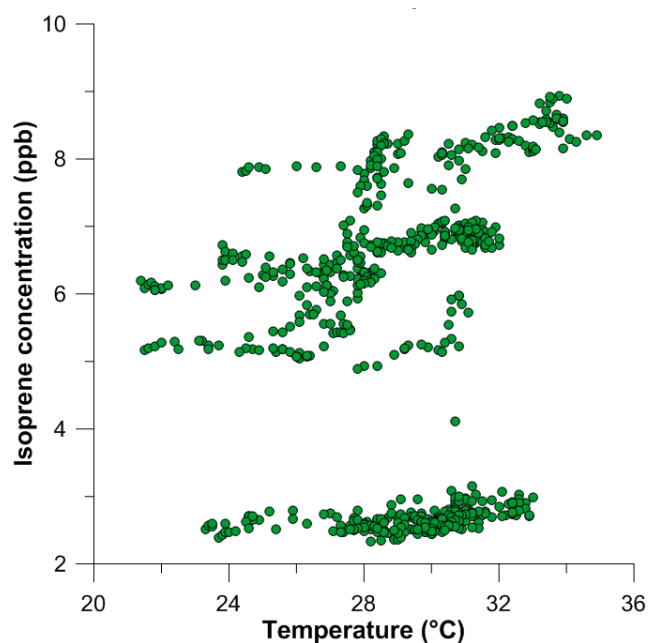
171

172

173

174

175

176

177

178



*Figure S12*. *Isoprene concentrations during daytime as a function of the temperature along the season.*

## S3. MEGANv2.1 Results

|  | MT* | Acetone | Acetaldehyde | MBO | DMS |
|---|---|---|---|---|---|
| Average | 58.62 | 16.363 | 10.629 | 10.248 | 0.477 |
| Range | 131.491 | 28.021 | 41.462 | 46.932 | 0.817 |

*\*MT: several key MTs are expected to be emitted from the nature park (see Sect. 2.1 in the main text), increasing in emission rate according to: myrcene (2%) > t-beta-ocimene (6%) >  3-carene (15%) > limonene (16%)> β-pinene (19%) > α-pinene (27%), and other MTs contributing 14%.*

## S4. Irregular meteorological conditions and mixing ratios during Julian days 257-260.

During Julian days 257-260, we measured irregularly high mixing ratios for several

VOCs (Fig. 2 in the main text) as well as for several measured trace gases (not shown

here). Because we also measured high wind speeds and low solar radiation intensity,

we hypothesized that the high mixing ratios were induced by higher than unusual

196 stable atmospheric conditions during summer. To investigate this hypothesis, we ran

197 the mesoscale weather research and forecasting (WRF) model, version 3.7.1. A

198 detailed description of the model can be found at http://www.wrfmodel.org/index.php.

199 A 1-km horizontal spacing domain was used with $190 \times 529$ grid points in the west–

200 east and south–north directions, respectively, covering the whole area of Israel, as

201 shown in Fig. S13.
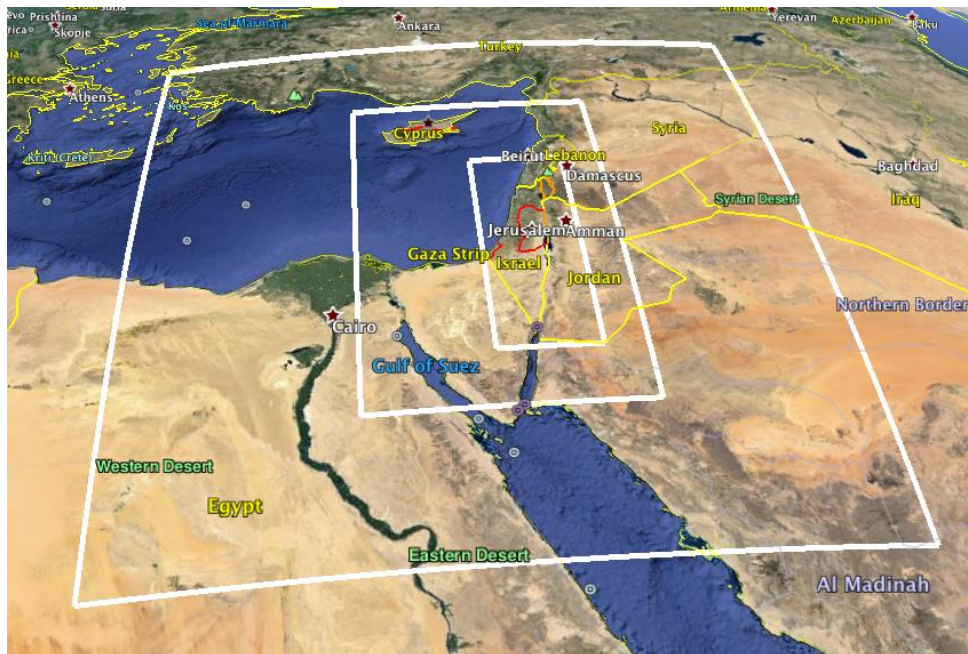
202



203 **Fig. S13.** *Map of the three nested domain grids of WRF simulations in the Eastern*
204 *Mediterranean (domain resolution: Domain 1 = 9 km, Domain 2 = 3 km, Domain 3 =*
205 *1 km). The WRF domain covers areas in southern Lebanon, Israel, West Syria, West*
206 *Jordan, and South Egypt. Background imagery from Google Earth.*

207

208 The 1-km resolution constitutes a compromise between optimal representation

209 of the terrain and land use, suitability of the planetary boundary layer (PBL)

210 parameterizations in the WRF model and computational requirements. The vertical

211 grid included 30 levels within the first 1 km above the ground. Initial and boundary

212 conditions were provided by NCEP GFS analysis

213 (https://rda.ucar.edu/datasets/ds083.2/), which has six hourly time resolutions and

214 $0.25^{o} \times 0.25^{o}$ horizontal resolution. The high vertical and horizontal resolution

215 enabled us to capture the local effect of terrain on meteorology.

216　　　　　　　Fig. S14 demonstrates relatively sharp decreases in the local PBL during 14-
217　　17 September, 2015, starting on each day in the late morning, which reinforces that
218　　the high mixing ratios measured on these days can be attributed to the shallow mixing
219　　ratios on these measurement days.
220
221
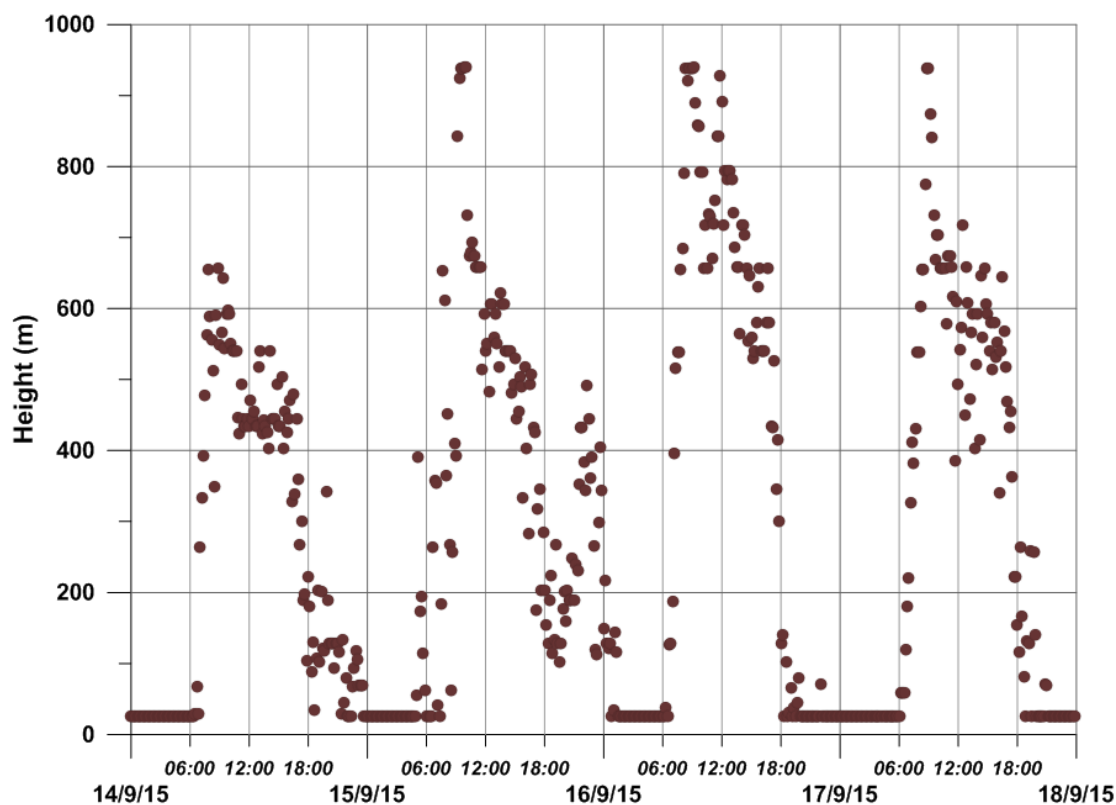


*Figure S14*. *Boundary layer height between 14-17 September, 2015. Induced by*
*irregularly meteorological conditions, the boundary layer height during this*
*measurement period was lower than during the other periods.*

**References**

Cappellin, L., Karl, T., Probst, M., Ismailova, O., Winkler, P. M., Soukoulis, C.,
　　　　Aprea, E., Märk, T. D., Gasperi, F. and Biasioli, F.: On quantitative
　　　　determination of volatile organic compound concentrations using proton
　　　　transfer reaction time-of-flight mass spectrometry, Environ. Sci. Technol.,
　　　　46(4), 2283–2290, doi:10.1021/es203985t, 2012.

235 de Gouw, J. A., Goldan, P. D., Warneke, C., Kuster, W. C., Roberts, J. M.,
236    Marchewka, M., Bertman, S. B., Pszenny, A. A. P. and Keene, W. C.:
237    Validation of proton transfer reaction-mass spectrometry (PTR-MS)
238    measurements of gas-phase organic compounds in the atmosphere during the
239    New England Air Quality Study (NEAQS) in 2002, J. Geophys. Res. Atmos.,
240    108(D21), doi:10.1029/2003JD003863, 2003.

241 de Gouw, J. and Warneke, C.: Measurements of volatile organic compounds in the
242    earth's atmosphere using proton-transfer-reaction mass spectrometry, Mass
243    Spectrom. Rev., 26(2), 223–257, doi:10.1002/mas.20119, 2007.

244 Lindinger, W., Hansel, A. and Jordan, A.: On-line monitoring of volatile organic
245    compounds at pptv levels by means of Proton-Transfer-Reaction Mass
246    Spectrometry (PTR-MS) Medical applications, food control and
247    environmental research, Int. J. Mass Spectrom. Ion Process., 173(3), 191–241,
248    doi:10.1016/s0168-1176(97)00281-4, 1998.